AIP Journal of Applied Physics

An inspection of force reduction in high force electromagnetic tweezers made of FeCo-V foil by laser cutting

La Chen, Andreas Offenhäusser, and Hans-Joachim Krause

Citation: Journal of Applied Physics **118**, 124701 (2015); doi: 10.1063/1.4931981
View online: http://dx.doi.org/10.1063/1.4931981
View Table of Contents: http://scitation.aip.org/content/aip/journal/jap/118/12?ver=pdfcov
Published by the AIP Publishing

An inspection of force reduction in high force electromagnetic tweezers made of FeCo-V foil by laser cutting

La Chen, Andreas Offenhäusser, and Hans-Joachim Krause[a)]
Institute of Bioelectronics (ICS-8/PGI-8), Forschungszentrum Jülich GmbH, 52425 Jülich, Germany

(Received 1 June 2015; accepted 17 September 2015; published online 29 September 2015)

One of the main goals in the design of magnetic tweezers is to obtain a high force output. In general, the force can be enhanced by adopting materials with high saturation magnetization and by using small sharp structures as magnetic pole tips. However, the practically achieved saturation forces are usually lower than predicted values. In this article, we inspect this issue in detail both by experiments and simulations. Our results show that the observed force reduction can be ascribed to two factors: magnetic performance deterioration near the cutting edges of the tips and a 3D geometrical effect. The high power laser used in cutting causes segregation and morphological roughness near the cutting edge. Moreover, the geometry of the magnetic tips plays an important role regarding the force behavior. As a matter of fact, there is a trade-off among high force, maneuverability, throughput, and manufacturing issues in practical design of magnetic tweezers. © *2015 AIP Publishing LLC*. [http://dx.doi.org/10.1063/1.4931981]

I. INTRODUCTION

Due to their simple architecture and extraordinary advantages, magnetic tweezers (MT) have become a popular scientific instrument in biology and biophysics. Because of their various special features, magnetic nanoparticles (MNPs) and microbeads are widely used as probes in MT.[1] One of these special features is the superparamagnetism which prevents particle agglomeration and thus paves the way for numerous applications.[2,3] Owing to the emerging novel magnetic particle synthesis techniques, the functionality and applications of MT have been expanded recently.[1] MT have been widely used in single molecules manipulation,[4,5] especially for stretching and twisting DNA molecules.[6] By adopting beads with high magnetization and optimized MT, the force on the probes can reach up to several nN,[7] which is comparable to forces in atomic force microscopy (AFM) used as force spectroscopy.[8] With the high forces achieved, MT are increasingly used in cell mechanics such as studies of transmembrane proteins,[9,10] of intracellular transport properties,[11] and of cell nuclei.[12] However, most of the high force MT were realized as single pole electromagnet, which limits their applicability because they do not allow manipulation of magnetic probes in different directions. In addition, usually only a single cell can be characterized at a time because the force drops quickly with the distance, so that the throughput is relatively low. Consequently, it will be beneficial to develop multi-pole high force MT which exhibit good maneuverability and high throughput. Our recently reported multi-pole MT shows good maneuverability and possesses a large workspace.[13]

It is well known that the output force of MT can be enhanced by using beads with high magnetization or by generating a high magnetic field gradient at the bead's position.[7,13] Usually, the magnetization can be improved by adopting large size MNPs embedded in the probe bead and a high volume ratio of magnetic material in the bead. However, this is compromised by the magnetic properties, such as coercivity, and by coating stability.[14,15] In order to generate a high magnetic field gradient, two main methods are used: (1) adopting soft magnetic materials with high saturation magnetization M_s, and (2) employing small sharp structures.[13,16] FeCo alloys, which exhibit high M_s, high Curie temperature, and low magnetocrystalline anisotropy, are ideally suited for applications requiring high flux density.[17] Although binary FeCo alloys have the highest saturation magnetization, they are limited to use in many applications on account of their brittleness. With the addition of vanadium as in industrial production, the workability of these alloys can be improved without decreasing the magnetization too much. With photolithographic technology and electro-deposition, small magnetic structures can be realized.[16,18] However, the material performance reported for thin electroplated layers[19–21] is usually below the values given for bulk material.[22] Moreover, the practical performance is also deteriorated because of the thickness effect.[23] The achievable force reduces with decreasing tip thickness. Another method to fabricate magnetic components with specified shape is using commercial material with industrial manufacturing process, such as punching, laser cutting, and wire electrical discharge machining. It is well known that cutting strain deteriorates the magnetic properties of electrical steel sheets in the area near the cutting edge.[24,25] However, the effect of laser cutting on the magnetic properties of FeCo alloys has not been reported yet. In this paper, we discuss the laser cutting effect and the geometry effect on the force properties of MT. Our results provide general guidelines for the design of high force MT with a large workspace to achieve high throughput.

[a)]Author to whom correspondence should be addressed. Electronic mail: h.-j.krause@fz-juelich.de.

II. MATERIALS AND METHODS

Our MT setup consists of a main hexapole yoke and a fluidic cell with magnetic tips. A schematic is presented in Fig. 1. The hexapole yoke is made of FeNi alloy (PERMENORM® 5000 H2, Vacuumschmelze GmbH & Co. KG, Germany). The fluidic cell includes 3 magnetic tips made from 100 μm thick FeCo-V foil (VACOFLUX® 50, Vacuumschmelze GmbH & Co. KG, Germany), which has a saturation magnetization M_s of 2.35 T. As shown in Fig. 1, the workspace is encircled symmetrically by the magnetic tips. The main yoke parts and the tips in the fluidic cell were cut by laser to form the designed geometry and were magnetically annealed under dry hydrogen atmosphere (manufactured by SEKELS GmbH, Germany). In order to get the desired configuration, the individual magnetic tips were aligned and pre-fixed on a cover slip under microscope with a small amount of slowly setting glue. Auxiliary lines were used in the alignment process with a customized LabVIEW program (National Instruments, USA). After the glue dried out, a glass ring was fixed on the cover slip with polydimethylsiloxane (PDMS, Sylgard 184, Dow Corning Corporation, USA). With the help of capillary force, the PDMS flows to fill the gap between the tips and the cover slip. Thanks to the good elasticity of PDMS, the tips are durable to high force operation. In order to assess the properties of tips, the magnetic forces on magnetic beads were measured by analyzing the viscous drag according to Stokes' formula. In this work, Dynabeads® M-270 Carboxylic Acid (Thermo Fisher Scientific, Inc., USA) with a diameter of 2.8 μm were used. All force simulations are based on the magnetization of this bead.[13]

A high viscosity fluid made from 95% glycerol (99.0%, Alfa Aesar GmbH, Germany) mixed with 5% water was used. The ratio of viscous fluid to bead solution was 200:1. The viscosity of this solution was calibrated at the same low force by dragging the beads in a lower viscosity solution of diethylene glycol (DEG, puriss, 99.0%, Sigma-Aldrich, USA). The viscosity of DEG was measured by a viscosity meter (microVISC, RheoSense, Inc., USA). In order to reduce the effect of ambient temperature change, the experiments with glycerol were done immediately after DEG dragging. Before every experiment, 0.2 ml of the mixed solution was injected into the fluidic cell with a pipette. After 10 min of sedimentation, drag experiments were done. The particle position was tracked with a 2D normalized cross-correlation algorithm.[13]

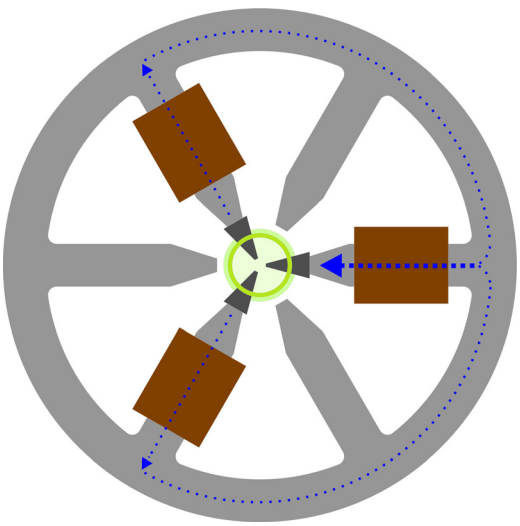

FIG. 1. Schematic of magnetic tweezers. The main yoke, magnetic tips, cover slip, glass ring, and coils are shown in light gray, dark gray, light green, green, and brown, respectively. The unused coils at the other three fingers are not shown. Blue dashes indicate the magnetic flux when the right pole is employed as the main pole. This drawing is not to scale.

In order to model the tips material effect, we inspected tips with different magnetic properties using finite element simulation (COMSOL Multiphysics, Magnetic Fields module, COMSOL, Inc., USA). The default magnetic insulation boundary condition was applied to the external boundaries. The B-H data of magnetic materials were adopted from the measurement results supplied by the manufacturer. Here, we define the positive coil current as injecting magnetic flux into the workspace, for example, the right coil in Fig. 1. For the purpose of decreasing magnetic flux leakage, the sum of the three active coil currents was always restricted to zero. In this work, the coil current always refers to the positive current of the main source coil. Accordingly, each of the other two bypass coils was supplied with half of this current at opposite polarity. The morphology of the magnetic tips was characterized by scanning electron microscope (SEM) (Magellan 400, Nanolab Technologies, USA) equipped with energy dispersive x-ray spectroscopy system (EDS) for element analysis. Only Fe, Co, and V elements were analyzed, and the measured signal intensities were normalized. The composition on each site was measured 3 times.

III. RESULTS AND DISCUSSION

A. Morphology and segregation in area near cutting edge

In contrast to traditional mechanical punching, laser beam machining has the virtue of a small heat-affected zone (HAZ), precision cutting, and flexibility. It is widely applied to all kinds of materials machining. The high density energy from the laser removes material by heating until the material is molten, evaporated, or chemically degraded.[26] Because of the non-contact cutting, this process avoids shearing deformation at the cutting edges. However, the high temperature shock from the laser pulse can modify the microstructure in area near the cutting edge of the material, which will induce some degree of deterioration in magnetic performance.[27]

In order to inspect the effect of laser cutting, the morphology of the tips after cutting was characterized by SEM. The tips were cut with a design width of 60 μm from a 100 μm thick sheet. As shown in Fig. 2(a), the surface planar slip texture of the tip indicates that the material is partially ordered in its crystal structure.[17] In general, the laser spot has a very high energy density in the center, and the HAZ changes quickly in space and time.[27] During the cutting process, the tip's top surface melts at first. So the tip surface usually has a narrower width at the top than at the bottom surface. The vertical surface is a little rough after cutting, which is similar as in electrical steel cutting.[24] As can be

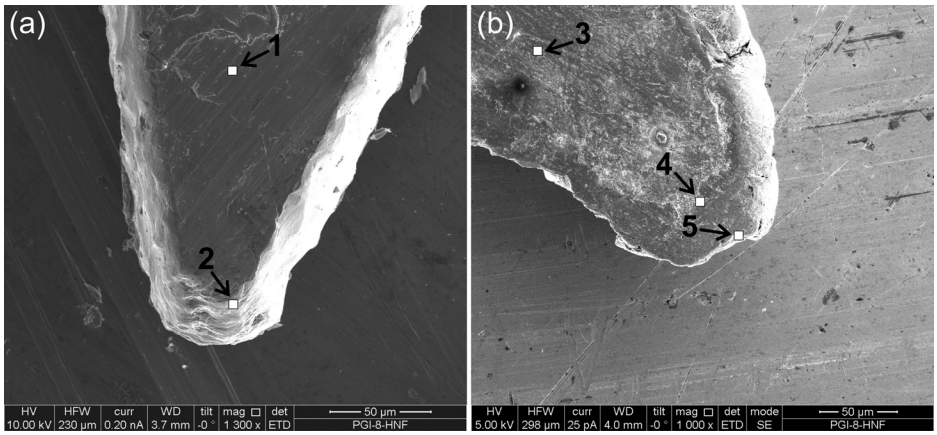

FIG. 2. Magetic tip after laser cutting: (a) top view and (b) bottom view (not the same tip).

clearly seen in Fig. 2(b), some molten material flowed down during cutting and solidified near the bottom edge. The composition at different sites marked as 1–5 in Figs. 2(a) and 2(b) was analyzed by EDS. The chemical atomic compositions of each point are listed in Table I. At sites 1 and 3 far away from the cutting edge, the composition is more consistent with the original ratio ($Fe_{49.1}Co_{49}V_{1.9}$). Due to a few micrometers penetration of EDS, the data deviate somewhat from the nominal composition. At the sites close to the cutting edge, the segregation becomes more obvious. The discrete compositions at the outer points 5 and 4 exhibit a higher cobalt content than the inner points 1 and 3. Except site 5, all sites have a higher ratio of vanadium than nominal. Moreover, a corrosion assay of our magnetic tips in cell culture medium also confirmed the vanadium enrichment at the surface (data not included here). And the vanadium composition in area near cutting edge has a large fluctuation. Besides, some oxygen was found by EDS in the area near the cutting edge, which may be evidence of some residual oxide after annealing.

B. The effect of material deterioration on magnetic force

Usually, FeCo-V alloys have a tendency to crystallize in γ phase (fcc) or α phase (bcc), depending upon the alloy composition and the heating process.[17] The segregation, such as the generation of a vanadium rich phase, could lead to a dilution effect due to non-magnetic precipitates that deteriorate the magnetic performance. In addition, the deviation from near-equatomic FeCo ratio causes atomic defects, enhances the magnetic anisotropy,[28] and reduces the permeability and saturation magnetization.[29] It is well known for Fe-Si electrical steels that the laser cutting induces stress in the area near the cutting edge.[25] This large internal stress distributed over several grains can be released partly during the annealing process. The residual stress tends to induce additional magnetic anisotropy and hence a lower permeability, and increases the coercive field. Compared to electrical steel, FeCo based alloys are usually more sensitive to strain because of a higher magnetostriction value. Although recrystallization takes place during annealing, the crystal structures near the cutting edge cannot recover totally at the annealing temperature (800–820 °C) recommended by the material vendor.

TABLE I. Element composition at different sites.

Inspection site	Fe (at. %)	Co (at. %)	V (at. %)
1	46.2 ± 0.67	49.17 ± 0.71	4.81 ± 0.24
2	40.51 ± 0.72	49.51 ± 0.67	9.98 ± 0.28
3	44.83 ± 0.77	49.82 ± 0.73	5.35 ± 0.26
4	39.63 ± 0.82	55.35 ± 0.78	5.01 ± 0.28
5	38.01 ± 0.90	60.85 ± 0.85	1.15 ± 0.23
Average[a]	45.14 ± 2.84	50.33 ± 4.08	4.53 ± 3.76

[a]Statistics on 36 sites on 20 μm layer near cutting edge from 9 tips. 3 sites with Vanadium >20% are not included.

In order to model these effects on the force output of MT in 2D simulation, the tips were divided into a bulk part and a layer near the cutting edge. In the case of 3 poles MT, the maximum magnetic field or force can be achieved when the width of tips have the same dimension as the radius of the workspace.[13] Here, both r and w equal 60 μm, as depicted in Fig. 3(a). Depending on the annealing time and temperature, the grain size of FeCo-V alloy ranges from few to dozens of μm, and the coercivity usually decreases with the size of the grains.[30] Although the area practically affected by laser cutting may be larger than one grain, we modeled the affected layer with thicknesses d of 10 μm and 20 μm, as shown in Fig. 3(a). The experimental magnetization (B-H) curve was fitted to a piecewise Langevin function, as given in Eq. (1). The parameters a and M_s are mainly related to the permeability and saturation magnetization, respectively. The parameters H_i and M_i are adjusted to join the low magnetic field section and the Langevin function. The B-H fitting curve for $H < H_i$ was adopted directly from the experimental data. The experimental B-H curve and the fitting result are shown in Fig. 3(b). The values adopted from the fitting result are a = 53.82, $M_s = 2.2$ T, $H_i = 22.76$ A/m, and $M_i = 0.0456$ T

$$M(H) = M_s\left(\coth\left(\frac{H-H_i}{a}\right) - \frac{a}{H-H_i}\right) + M_i, \quad H > H_i. \tag{1}$$

In order to simulate the magnetization of the affected areas, parameters a, M_s, and M_i were tuned. For the deterioration of M_s, the original M_s and M_i in Eq. (1) were multiplied by a reduction factor. The B-H curves at low H were

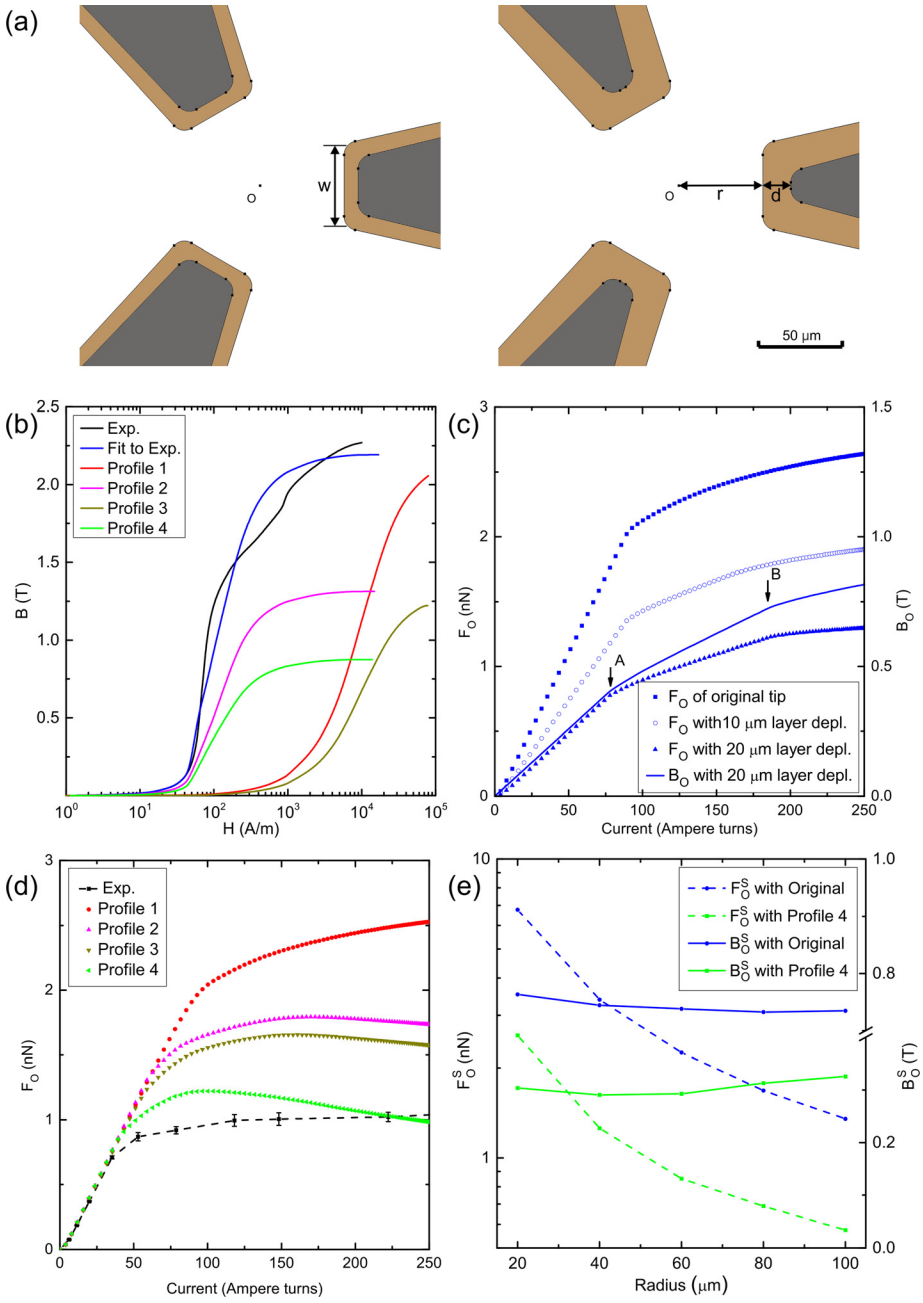

FIG. 3. (a) Simulation structures used for modeling the magnetization deterioration effect. The unaffected bulk is sketched in dark grey, the affected area near the cutting edge is shown in light brown. The central point of the workspace is marked as O. (b) Different tuned B-H curves used for simulating the layer near the cutting edge. (c) The simulated force-current curves for different geometries. Blue line represents the magnetic field of tips with 20 μm edge layer depleted. The knee points A and B are explained in the text. (d) Simulated force-current curves for different material properties in the 20 μm edge layer. The black curve shows a typical experimental result. (e) The saturation force and magnetic field for different workspace radii were calculated with original and tuned magnetic properties of the edge layer. The widths of tips were chosen to equal the workspace radius. For the structure with 20 μm wide tips, only a 10 μm thick edge layer was adopted.

reduced by the same factor. The B-H curve with M_s reduced to 0.6 times is plotted in Fig. 3(b) as Profile 2. The permeability can be tuned by the parameter a. As shown in Fig. 3(b), both parameters a and M_i in Profile 1 were reduced 100 times at $H > H_i$. As a simple approximation, the B-H at $H < H_i$ was modeled as a linear function only depending on M_i. The parameters for modeling are all listed in Table II.

As the first step, the outer layer of the tips was depleted and treated like air. The results are shown in Fig. 2(c). We can see that in all cases, the magnetic force at the central point O first increases linearly with the driving current. The linear relation between force and magnetic field can be explained by the magnetization of the bead. Due to superparamagnetism, the bead has a small linear magnetization range at magnetic fields <10 mT. The knee point of magnetization (the crossover to saturation) is low, around 50 mT.[13] So, the nonlinear force-current relation only exists at very low magnetic fields not shown in the figure. Beyond the knee point, the magnetic moment of the bead saturates very quickly; thus, the contribution to increasing magnetic force only comes from the increasing magnetic field gradient. Because of high magnetic flux output, the intact tips without

TABLE II. Reduction factors used for B-H tuning at cutting edge.

	$H > H_i$			
	a	M_s	M_i	$H < H_i$
Original[a]	1	1	1	Scale from expt.
Profile 1	0.01	1	0.01	Linear
Profile 2	1	0.6	0.6	Scale from expt.
Profile 3	0.01	0.6	0.006	Linear
Profile 4	1	0.4	0.4	Scale from expt.

[a]Fitting of experimental data.

depleted edge layer exhibit the highest slope and the highest saturation force. In the 20 μm depleted layer situation, the magnetic field at point O is shown in Fig. 3(c). There are two saturation points A and B. Point A corresponds to the magnetization saturation happening at the vortexes of the tips. When the saturation area expands with increasing current, the second knee point B emerges, at which the whole front area of the tip gets saturated. The progress of force follows well the magnetic field change. Beyond point B, the force does not increase any more with current. Using different tuned magnetic properties in the 20 μm thick edge layer, the corresponding force-current curves are presented in Fig. 3(d). Unlike the previous depleted edge layers, all force-current curves have the same slope. The force after saturation decreases a little in case of lower permeability. Compared to the permeability, the saturation magnetization M_s has a stronger effect on the high force. It is obvious that the experimental saturation force is very close to the tip with B-H property of Profile 4 in the edge layer. However, the saturation magnetization (0.88 T) here is much lower than the estimated value ($\sim$1.8 T) based on the average composition in Table I and the data shown in Ref. 17. In order to clarify this, three other contributing factors should be considered: (1) The permeability also has an important role on the saturation force, especially when the permeability of material is close to 1 at high magnetic field. (2) The real B-H data of the material in the HAZ is much more complicated than the formula adopted here. (3) In practice, the deterioration of the magnetic properties of the tips reduces with increasing distance from the cutting edge, unlike the uniform layer in our simulation model. As shown in Fig. 3(d), the experimental tip has a complex magnetic saturation behavior. There are three saturation stages. The first saturation stage is very short. We assume that it comes from the 3D structure. The area near the tip surface gets saturated first, and then the saturation area extends quickly into the surface layer. As shown in Fig. 3(d), when the saturation area extends more deeply into the bulk of the tip, the second stage appears. In experiment, because of permeability reduction, this progress is more like in Profile 3 situation slower than Profile 4. As in simulation, when the whole front tip gets saturated, more magnetic flux flows directly among the tips without passing through the workspace. So, the magnetic field gradient and the force in the workspace even start to decrease with increasing current. However, in the third saturation stage, the force in experiment still increases very slowly with current. We ascribe this to the strong domain pinning effect at crystal defects, caused by the thermal shock from the laser pulses.

As discussed in the introduction, the saturation force of MT can be enhanced by adopting a small sharp structure. The saturation force and magnetic field were calculated for different workspace radii, as shown in Fig. 3(e). In addition, the saturation forces with magnetic properties tuned with Profile 4 in 20 μm edge layer are also presented. As shown in the magnetic field plot, the saturation magnetic field at workspace center almost keeps constant close to 1/3 B_s of tip. With a closer distance among tips, higher magnetic field gradients and hence higher forces can be achieved. For example, when the radius is 40 μm, the saturation force achieved with the original tips is 3.38 nN, whereas the tip with tuned magnetic properties can only apply 1.26 nN. And the force ratio between original and tuned tips varies around 2.3–2.6.

C. The effect of tip geometry on magnetic force

Because of the focussing characteristics of a laser beam and the finite thickness of the tips, the effect from laser cutting is different in vertical direction. The structure of the 0.5 mm thick tip (microscope image not shown here) at the front is not as well defined as for the 0.1 mm thick tip. In experiments, the fluidic cell prepared with 0.5 mm thick tips exhibits an obvious remnant magnetization when coil current is turned off. When there is a large workspace among the tips, the effects from small local shape defects such as displacement, size deviation, and convex-concave roughness can be neglected. However, in case of a small workspace, the geometry of the tips usually has a strong effect on the force properties. In view of accuracy and maneuverability, the effective workspace of a real fluidic cell depends on the geometrical quality of its tips. A sample of a fluidic cell made of 0.1 mm tips is shown in Fig. 4(a). As can be seen, the real profiles have a small deviation from the symmetrical contours. Tip 1 has a width larger than 60 μm at the front edge. As seen in the inset image, there is an indentation at the front edge of the top surface. Tip 2 is sharper at the front than designed. At the front of tip 3, there is an obvious burr, which is a remnant of the molten material from cutting.

In order to revalue the impact of different profiles of the tips, we measured the force-current curves at the center of the workspace for every tip. At first, tip 2 was measured, then the tip 3 and tip 1. As in Fig. 4(b), before saturation, the forces of tip 2 and tip 3 agree very well with simulation. The force of tip 1 is little higher than that of tip 2 and tip 3. This may be attributed to the larger size of the tip. Besides, the viscosity of the solution is sensitive to temperature. After some time, the high coil current and the illumination light will induce a small temperature rise in the fluidic cell. It is obvious that all the experimental forces are a little bit higher than the simulated values for forces $<$100 pN (see Fig. 4(b)). We inferred that this results from an underestimation of the bead's magnetic moment at low magnetic fields. Moreover, all force directions change very little in the linear range. When the coil current increases to 50 A turns, the forces start to saturate. As mentioned before, there are three saturation stages. In the saturation stages, the magnetic field distribution among the tips begins to fluctuate lightly. As a result, the force directions also exhibit fluctuations. Compared to tip 1 and tip 3, the force direction fluctuation of tip 2 is larger. This can be deduced from the more irregular structures of tip 1 and tip 3. However, the force direction fluctuation with current change is relatively small and less than 9°. In order to evaluate the effect of tip profile on the force distribution in workspace, we adopted the contours of the tips for the 2D simulation, as depicted in Fig. 4(a). We also measured the force distribution on a 5×5 grid (x: from -20 μm to 20 μm and y: from -20 μm to 20 μm, each with 10 μm step). The results are shown in Fig. 4(c). In the upper left corner, the largest difference between experimental force

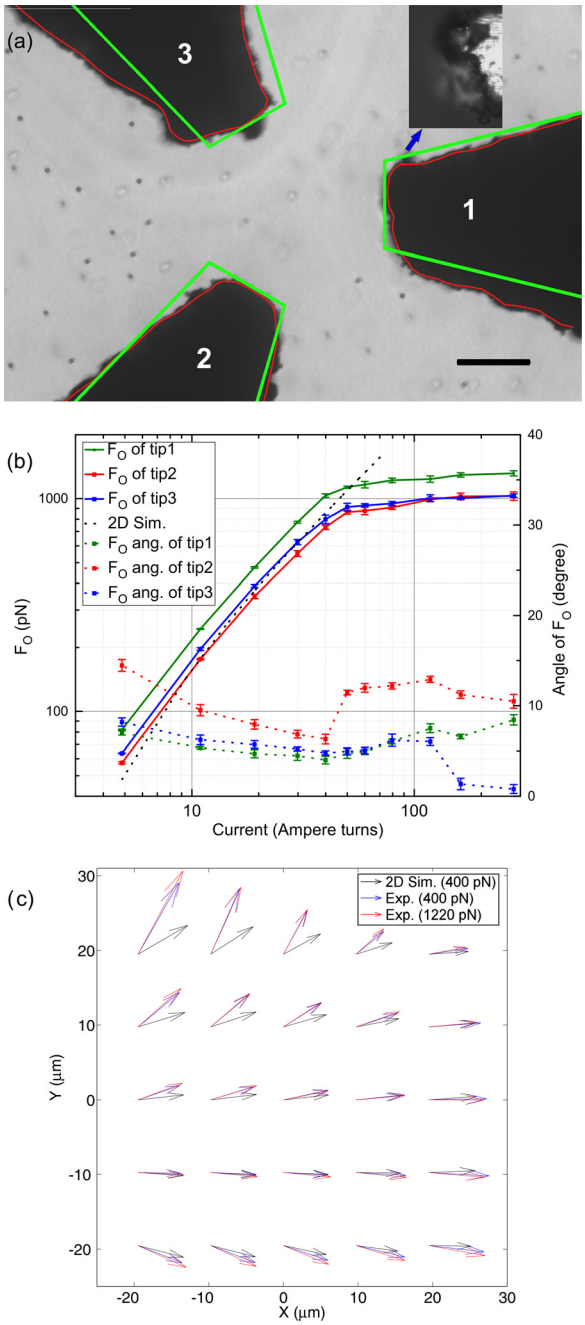

FIG. 4. (a) A fluidic cell with 60 μm workspace radius. The thick green line is the symmetrical contour. Red lines are used as the structure in 2D simulation. The inset figure shows the top surface of tip 1. The scale bar is 50 μm. (b) Force-current curves and force directions of different tips at workspace center O. (c) Force distribution in the central area of the workspace, with tip 1 as the main source tip. All force distributions are scaled to O.

and simulation can be noted, which comes from the extruded part at tip 3. The sharp structure has a strong impact on the local force. Except for a scaling factor, the force distribution changes very little in the experiment beyond saturation. However, compared to the simulation, the experimental force deflected away lightly to bypass tips in up and down area.

The observed difference between experimental and simulated force directions far away from deformed tip cannot be explained by the 2D profile of the tips. In 2D simulation, the vertical dimension is assumed to be infinite. In reality, all the tips have a finite thickness. The magnetic field bypassing along both sides of the tip will decrease the magnetic flux distribution in the workspace. So, 3D simulation is necessary for clarifying this. Because it requires heavy computational effort and it is hard to achieve convergence, we did 3D simulations only for single coil currents configuration. The magnetic properties of the tips are adopted as the fitted B-H curve describing experimental data. As shown in Fig. 5(a), except for the middle plane, the force vectors pointing to the source tip have vertical components, which become more obvious far away from middle plane and close to the source tip. The force in the bottom half space is symmetrical to the top half space. The force distributions in plane for different situations are shown in Fig. 5(b). We can see that all force distributions are very similar near the source tip. As in the experiment, the forces at the corners away from the source tip are deflected more to the bypass tips, which is more obvious far away from the middle plane. Besides, the force errors in the plane 5 μm above the top surface of tip caused by displacement and width deviation of tips are shown in Figs. 5(c) and 5(d). We can see that all force errors are local. The force error decreases with increasing distance from the deformed tip. The defect on one side of tip has only very little effect on the force on the other side, not shown in this figure. This agrees with the experimental force depicted in Fig. 4(c). The obvious notch on the top surface of tip 1, as seen in the inset in Fig. 4(a), has little effect on the force distribution in the middle plane.

So far, we have discussed the effect of tip geometry on the direction of force. As discussed in Section III B, besides the permeability and M_s, the strength of force also depends on the geometry of the tips. As shown in Table III, with 40 A turns coil current, the force at central point decreases with the thickness of the tip. The force with 100 μm thick tips is a little higher in 3D simulation (1076 pN) than in 2D simulation (860 pN) and in the experiment, which may come from the different configurations. In order to avoid convergence problems due to nonlinear material properties, the forces of 50 μm and 25 μm tips at 40 A turns are scaled from 30 and 20 A turns, respectively. In a plane 5 μm above the top surface plane, the force at central point also decreases with the tip thickness, although the F_H/F_O increases a little. Besides, the vertical component (F_V/F_H) also decreases with thickness. Therefore, we can conclude that the force is reduced if the tip is too thin. This result was also observed in Ref. 23. When the distance among tips is comparable to the thickness of the tips, the force reduction from this 3D geometrical effect becomes negligible. This property is similar as in permanent magnet MT.[31] However, except a scaling factor, the

TABLE III. The tip thickness effect on force.[a]

Thickness (μm)	F_O (pN)	F_H (pN)	F_H/F_O	F_V/F_H
100	1076.4	759.95	0.71	0.64
50	686.97	533.74	0.77	0.57
25	420.72	368.74	0.88	0.46

[a]F_H refers the force component in plane 5 μm above tip surface. F_V refers the force component in vertical direction.

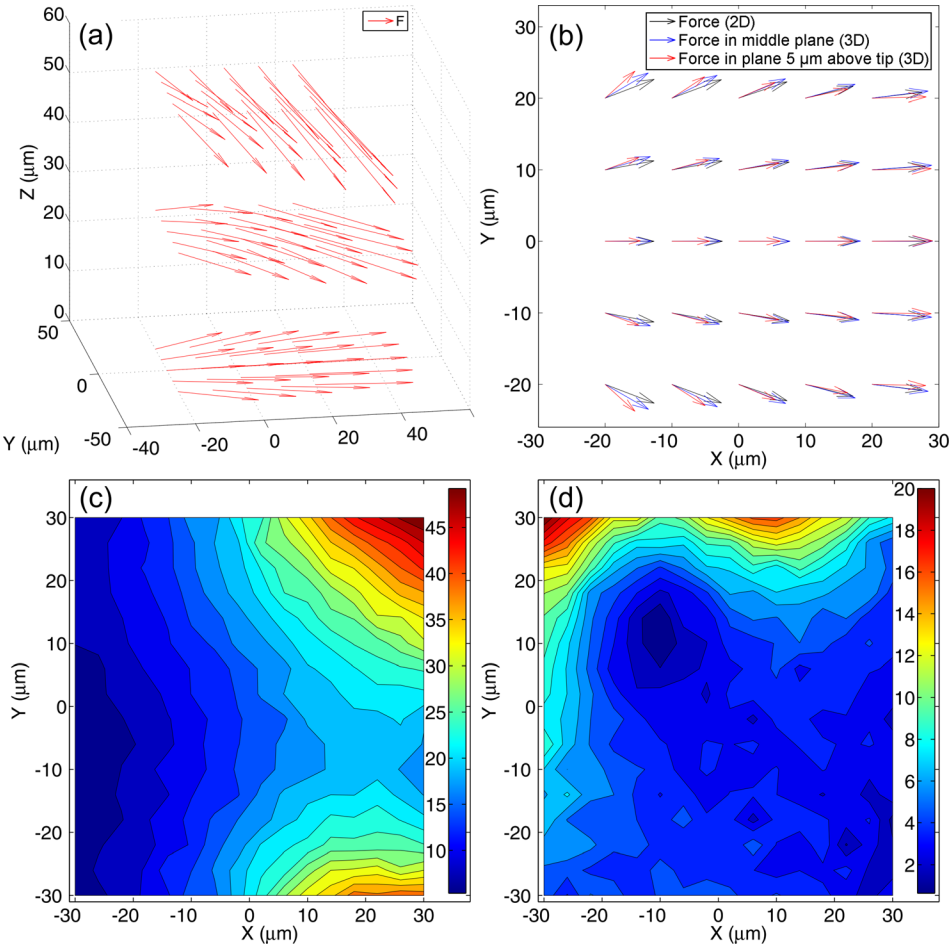

FIG. 5. (a) Force distributions at top plane, intermediate plane and middle plane. The right tip is set as source tip. The coil current is set to 40 A turns. (b) Force distributions for different situations. The forces are scaled to the central point. (c) The force error caused by 20 μm displacement along y axis on the right tip. (d) Force error caused by left top tip, which has a width of 40 μm.

force distribution of thinner tips in 3D simulations is more close to that of 2D simulation, which means we can adopt 2D simulation in case of structures with a small aspect ratio without inducing too much error.

IV. SUMMARY

In conclusion, the laser cutting has an important effect on the magnetic properties and morphology of outer layer near the cutting edges of the tips. The induced reduction in saturation magnetization and permeability plays a vital role on the high force reduction in MT. Compared to the permeability, the reduction of M_s has a stronger effect. The MT force also may be reduced due to geometrical effects such as its small thickness and narrowing of the tip after cutting. Based on these findings, the optimized MT presented here can apply a force higher than 1 nN on a 2.8 μm superparamagnetic bead, which is comparable to the results of Ref. 23 and amounts to about half of the force reported for single pole magnet MT.[7] However, our MT has a large workspace of $60 \times 60\ \mu m^2$, which allows to achieve high throughput for parallel measurements.

With the optimized MT, the force at the corners of workspace is more deflected toward the bypass tips, which reduces the maneuverability in these areas. There are also higher vertical force components in planes away from the middle plane of the tips, which may be useful for some applications, for example, if one wants to stretch DNA molecules. In addition, tip shape defects such as burrs and size deviation have strong effects on the local force. However, with optimized cutting process, both the morphology and magnetic performance of tips are expected to improve.

ACKNOWLEDGMENTS

This work was performed in part at the Helmholtz Nanoelectronic Facility of Forschungszentrum Juelich. We thank Dr. Swen Graubner (SEKELS GmbH) for beneficial discussion. La Chen acknowledges support by the China Scholarship Council (No. 201206890062).

[1]D. Kilinc and G. U. Lee, Integr. Biol. **6**, 27 (2014).
[2]A.-H. Lu, E. L. Salabas, and F. Schüth, Angew. Chem., Int. Ed. **46**, 1222 (2007).
[3]Q. A. Pankhurst, J. Connolly, S. K. Jones, and J. Dobson, J. Phys. D: Appl. Phys. **36**, R167 (2003).
[4]A. D. Rio, R. Perez-Jimenez, R. Liu, P. Roca-Cusachs *et al.*, Science **323**, 638 (2009).
[5]R. Watanabe, R. Iino, and H. Noji, Nat. Chem. Biol. **6**, 814 (2010).
[6]I. D. Vlaminck and C. Dekker, Annu. Rev. Biophys. **41**, 453 (2012).
[7]P. Kollmannsberger and B. Fabry, Rev. Sci. Instrum. **78**, 114301 (2007).
[8]K. C. Neuman and A. Nagy, Nat. Methods **5**, 491 (2008).
[9]M. A. Hemphill, B. E. Dabiri, S. Gabriele, L. Kerscher *et al.*, PLoS One **6**, e22899 (2011).
[10]P. Roca-Cusachs, A. D. Rio, E. Puklin-Faucher, N. C. Gauthier *et al.*, Proc. Natl. Acad. Sci. U.S.A. **110**, E1361 (2013).
[11]J. Mahowald, D. Arcizet, and D. Heinrich, Chem. Phys. Chem. **10**, 1559 (2009).
[12]A. H. B. de Vries, B. E. Krenn, R. van Driel, V. Subramaniam, and J. S. Kanger, Nano Lett. **7**, 1424 (2007).
[13]L. Chen, A. Offenhäusser, and H.-J. Krause, Rev. Sci. Instrum. **86**, 044701 (2015).

[14]A. G. Kolhatkar, A. C. Jamison, D. Litvinov, R. C. Willson, and T. R. Lee, Int. J. Mol. Sci. **14**, 15977 (2013).
[15]K. Landfester and L. P. Ramírez, J. Phys.: Condens. Matter **15**, S1345 (2003).
[16]A. H. B. de Vries, J. S. Kanger, B. E. Krenn, and R. van Driel, J. Microelectromech. Syst. **13**, 391 (2004).
[17]R. S. Sundar and S. C. Deevi, Int. Mater. Rev. **50**, 157 (2005).
[18]C.-H. Chiou, Y.-Y. Huang, M.-H. Chiang, H.-H. Lee, and G.-B. Lee, Nanotechnology **17**, 1217 (2006).
[19]J. Y. Park and M. G. Allen, J. Micromech. Microeng. **8**, 307 (1998).
[20]X. Liu, G. Zangari, and M. Shamsuzzoha, J. Electrochem. Soc. **150**, C159 (2003).
[21]I. Shao, P. M. Vereecken, C. L. Chien, R. C. Cammarata, and P. C. Searson, J. Electrochem. Soc. **150**, C184 (2003).
[22]Vacuumschmelze GmbH&Co. KG, *Soft Magnetic Materials and Semi-finished Products* (Vacuumschmelze GmbH & Co. KG, Germany, 2002).
[23]A. H. B. de Vries, B. E. Krenn, R. van Driel, and J. S. Kanger, Biophys. J. **88**, 2137 (2005).
[24]Y. Kurosaki, H. Mogi, H. Fujii, T. Kubota, and M. Shiozaki, J. Magn. Magn. Mater. **320**, 2474 (2008).
[25]P. K. Klimczyk, P. Anderson, A. Moses, and M. Davies, IEEE Trans. Magn. **48**, 1417 (2012).
[26]A. K. Dubey and V. Yadava, J. Mater. Process. Technol. **195**, 15 (2008).
[27]A. Belhadj, P. Baudouin, and Y. Houbaert, J. Magn. Magn. Mater. **248**, 34 (2002).
[28]R. C. Hall, J. Appl. Phys. **31**, S157 (1960).
[29]R. M. Bozorth, *Ferromagnetism*, 5th ed. (D. Van Nostrand Company, Inc., USA, 1951), p. 194.
[30]R. H. Yu, S. Basu, Y. Zhang, A. Parvizi-Majidi, and J. Q. Xiao, J. Appl. Phys. **85**, 6655 (1999).
[31]J. Lipfert, X. Hao, and N. H. Dekker, Biophys. J. **96**, 5040 (2009).